

Article

Fate of Copper in Saline–Alkali Soil with Long-Term Application of Biogas Residue

Binhao Liu ¹, Shengxiao Wang ^{1,2}, Pengcheng Dong ¹, Xinzhe Zhang ¹, Long Zhang ¹, Chen Chen ¹ , Xihui Xu ¹ , Yan Xia ¹, Zhenguo Shen ^{1,3}, Liang Shi ^{1,4,5} and Yahua Chen ^{1,3,4,5,*}

¹ College of Life Sciences, Nanjing Agricultural University, Nanjing 210095, China

² China Tobacco Shandong Industrial Co., Ltd., Jinan 250104, China

³ Jiangsu Collaborative Innovation Center for Solid Organic Waste Resource, Nanjing Agricultural University, Nanjing 210095, China

⁴ National Joint Local Engineering Research Center for Rural Land Resources Use and Consolidation, Nanjing Agricultural University, Nanjing 210095, China

⁵ The Collaborated Lab of Plant Molecular Ecology (between College of Life Sciences of Nanjing Agricultural University and Asian Natural Environmental Science Center of the University of Tokyo), College of Life Sciences, Nanjing Agricultural University, Nanjing 210095, China

* Correspondence: yahuaachen@njau.edu.cn

Abstract: The retention of copper (Cu) in saline–alkali soil (SAS) during long-term application of biogas residue (BR) with a high concentration of Cu raises concerns. In this work, the fate of Cu was detected using adsorption isotherms, scanning electron microscope—energy dispersive spectrometer, Fourier transform infrared spectrometer, X-ray diffraction, isothermal titration calorimetry, X-ray photoelectron spectroscopy, and microzone X-ray fluorescence spectrometer. The results showed that the main groups for Cu adsorption by SAS and BR were carboxyl, hydroxyl, amide and amine. The adsorption of Cu by the carboxyl group was entropy–enthalpy co-driven ($|\Delta H| < |\Delta S|$, $\Delta H < 0$). The adsorption of Cu by the amine group was entropy-driven ($|\Delta H| > |\Delta S|$, $\Delta H > 0$). The adsorption of Cu on the SAS and BR was achieved by organic matter rather than minerals. The degradation of BR in the SAS increases the content of Cu adsorption groups such as carboxyl and amine groups, and Cu was adsorbed on the surface or inside SAS through organic groups. This study provides further theoretical support for the application of BR in SAS.

Keywords: copper fate; biogas residue; complexation; redox; degradation; adsorb



Citation: Liu, B.; Wang, S.; Dong, P.; Zhang, X.; Zhang, L.; Chen, C.; Xu, X.; Xia, Y.; Shen, Z.; Shi, L.; et al. Fate of Copper in Saline–Alkali Soil with Long-Term Application of Biogas Residue. *Agriculture* **2023**, *13*, 915. <https://doi.org/10.3390/agriculture13040915>

Academic Editor: Bin Gao

Received: 6 April 2023

Revised: 19 April 2023

Accepted: 20 April 2023

Published: 21 April 2023



Copyright: © 2023 by the authors. Licensee MDPI, Basel, Switzerland. This article is an open access article distributed under the terms and conditions of the Creative Commons Attribution (CC BY) license (<https://creativecommons.org/licenses/by/4.0/>).

1. Introduction

Copper (Cu)-contaminated biogas residue (BR) produced in the biogas digestion process of Cu pollution remediation plants can be used to improve the soil utilisation rate and accomplish the recycling of organic waste. Soil salinisation is becoming increasingly serious. Saline soils are characterised by high salt ion concentrations, high pH values, low organic matter content and poor soil structure, which are not conducive to agricultural activities and therefore many saline soils are underutilised [1,2]. The application of digested obtained after anaerobic fermentation of heavy metal-contaminated soil phytoremediation plants to SAS is, therefore, an excellent way to post-treat remediation plants. In the application process of Cu-contaminated BR, the migration mechanism of Cu in saline–alkali soil (SAS) has yet to be explored. The application of synchrotron radiation [1], electron microscope [3], X-ray absorption spectroscopy [4] and other physical research methods [5,6] in the field of soil environment provides more intuitive research methods for the occurrence and migration of heavy metals in soil. In the process of sludge improvement of farmland soil, the decomposition of organic matter was found to be the key factors of Cu [7–9]. The transformation of Cu(II) and Cu(I) is affected by the redox reaction of organic matter [10,11].

In this study, in order to study the migration and transformation of Cu during the continuous application of BR in saline–alkali soil (SAS), methods such as adsorption isotherms,

scanning electron microscope–energy dispersive spectrometer (SEM–EDS), Fourier transform infrared spectrometer (FTIR), X-ray diffraction (XRD), isothermal titration calorimetry (ITC), X-ray photoelectron spectroscopy (XPS), and microzone X-ray fluorescence spectrometer (Micro-XRF) analysis were adopted to explore the migration mechanism of Cu. The aim of this study was to (1) compare the adsorption properties of Cu on SAS and BR, (2) test chemical environment changes of Cu adsorbed in SAS and BR, (3) study the combination mode of Cu on the surface of SAS and BR, (4) study the changes of Cu and main functional groups during the continuous application of BR in SAS and (5) Cu distribution during continuous application of BR.

This study is important for improving the technical system of phytoremediation of contaminated soil, and it can also provide a technical approach for the remediation and exploitation of problematic soils (SAS).

2. Materials and Methods

2.1. Saline–Alkali Soil and Biogas Residue

The SAS was taken from the Dafeng coastal beach in Jiangsu province (32°59′51″ N, 120°49′21″ E). Basic information of the soil for the experiment was published in a previous article [12]. The Cu-contaminated BR was collected from the anaerobic digestion of Cu pollution remediation plants *Elsholtzia splendens*. The SAS was mixed with 2% Cu-rich BR for one season (2% × 1), two seasons (2% × 2), three seasons (2% × 3), four seasons (2% × 4) and five seasons (2% × 5); wheat and soybean were rotated at each growing season.

To study the influence of organic matter in saline alkali soil, we refer to the hydrogen peroxide method [2] for the removal of organic matter from soil and enhance the method. Specific operations are: First, to 5 g of 100-mesh sieved saline–alkali soil, 100 mL of deionised water were added. Then, H₂O₂ (30%) was added continuously and stirred constantly until no bubbles emerged. The mixture was centrifuged for 12 min at 8000 rpm. After filtration, the solids were cleaned five times with deionised water, then dried at 45 °C. After the above treatment, 97.46% of the organic carbon in SAS can be removed (Table S9). Therefore, it is used as organic-free SAS.

2.2. Adsorption Isotherms of Cu

SAS, organic-free SAS and BR were dried, crushed and screened through a 100-mesh sieve. From each experimental sample, 1 g was taken and 10 mL Cu²⁺ adsorption solution was added. Five replicates were established for the experiment, and deionised water was used as the blank. The mixture was placed in a horizontal shaker at 25 °C for 24 h, after which the mixture was centrifuged at 8000 rpm for 12 min. The supernatant was filtered in the centrifuge tube, and the content of Cu was determined by AAS (Nov AA400, Analytik Jena Co., Ltd., Jena City, Freistaat Thüringen, Germany). The Cu²⁺ adsorption solution was Cu(NO₃)₂ with the concentrations of 1, 2, 5, 10, 20, 50, 100, 200, 500, 1000, 2000, 5000 and 10,000 mg/L. Finally, 0 mg/L solution was deionised water.

2.3. Analytical Methods

Of the items measured, the Bruker D2 PHASER was used for the XRD measurements. Determination conditions were CuK_α target radiation, a scanning speed 2°/min and a scanning range of 3–60°. FTIR measurements were performed using Nicolet iS5 infrared spectrometers. The samples were scanned in the range 400–4000 cm^{−1} with a setting of 16 scans and the spectra were registered using a Nicolet iS5 infrared spectrometer with a resolution of 4 cm^{−1}. The ITC measurement was carried out using a MicroCal iTC200 isothermal titration micro-calorimetric instrument, with the experimental temperature set at 25 °C. The XPS assay was carried out using the Scanning XPS Microprobe PHI Quantera. Analysis area was 2.0 × 2.0 μm (length × width), the full spectrum scanning energy was 280 eV, the fine spectrum scanning energy was 69 eV, and the element binding energy by C 1s correction (284.8 eV). The Micro-XRF instrument was a microzone X-ray fluorescence spectrometer (M4 tornado, Bruker, Germany). The SEM–EDS instrument is

a scanning electron microscope and energy dispersive spectrometer (HITACHI, S-3000N, Tokyo, Japan). The detailed information of the determination of XRD, FTIR, ITC, XPS, Micro-XRF and SEM–EDS were shown in Supplementary Materials (S1).

3. Results and Discussion

3.1. Basic Properties of Soil

The basic properties of the SASs were shown in Figure 1. With the continuous application of BR, the pH in the soil decreased continuously from 8.18 ± 0.12 to 7.40 ± 0.08 . The content of organic matter in soil was $2.22 \pm 0.18\%$, and the continuous application of BR increases the content of organic matter in soil to $3.88 \pm 0.19\%$. Despite five consecutive crop seasons of BR application, the soil Cu concentration of the SAS (71.3 ± 5.4 mg/kg) remained below the limits of the national standard (GB 15618-2018, 100 mg/kg Cu, pH 6.5–7.5) (Figure 1c). After four seasons, most of the Cu was in the sulphides/organic matter fraction and residual fraction, the related research results in our laboratory [13].

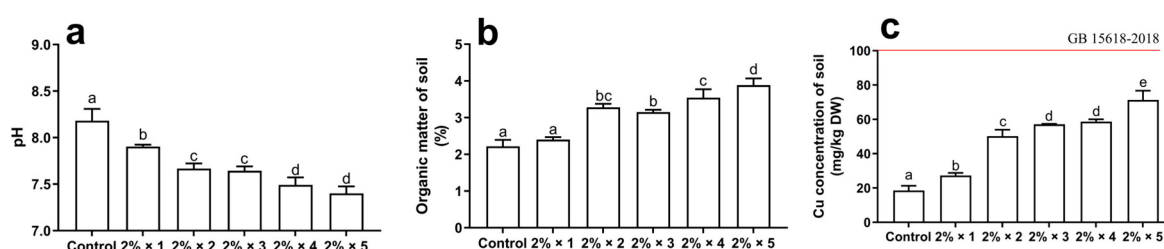


Figure 1. The pH (a), organic matter content (b) and Cu content (c) of the SASs (control) and application of 2% BR for one season, two seasons, three seasons, four seasons, five seasons. Red solid line indicates the concentration of soil Cu limited in GB15618-2018. Data are means \pm SD of three biological replicates, with different letters in the same soil treatment indicating significant ($p < 0.05$) differences according to Tukey's test.

3.2. XRD Analysis for Saline–Alkali Soil

In order to characterise the mineral types and relative contents of SAS, and to explore the influence of organic matter in SAS on the mineral types and relative contents, the X-ray diffraction patterns of SASs and organic-free SAS were tested (Figure 2). According to the analysis of the diffraction characteristics of minerals, there are seven mineral components in SAS: quartz, illite, struvite, pyroxene, calcite, sodalite and hornblende. The peak of the diffraction characteristics is shown in Table S1. In the process of removing organic matter from SASs, four mineral components (struvite, calcite, sodalite and hornblende) lower relative contents disappeared, forming berlinite and struvite-K with relative contents of 18.94 and 3.18%, respectively. Illite is a layered silicate mineral with high cation exchange capacity and specific surface area and strong adsorption capacity of heavy metals [14,15]. Struvite contains N, P, Mg and other nutrients needed by plants [16], and it has the potential to stabilise heavy metals in soil [17]. Pyroxene is a silicate mineral produced by reaction of CaO, MgO and SiO₂ at high temperature [18]. Calcite plays an essential role in the utilisation of heavy metals and is an important environmental mineral [19]. In the process of removing organic matter from SAS, berlinite and struvite-K are formed. Berlinite is the most stable and nonporous phase of all the polymorphs of aluminophosphates [20]. Among them, the diffraction peak of struvite is shifted to a high angle, indicating that struvite-K is formed by K⁺ entering the struvite lattice [21].

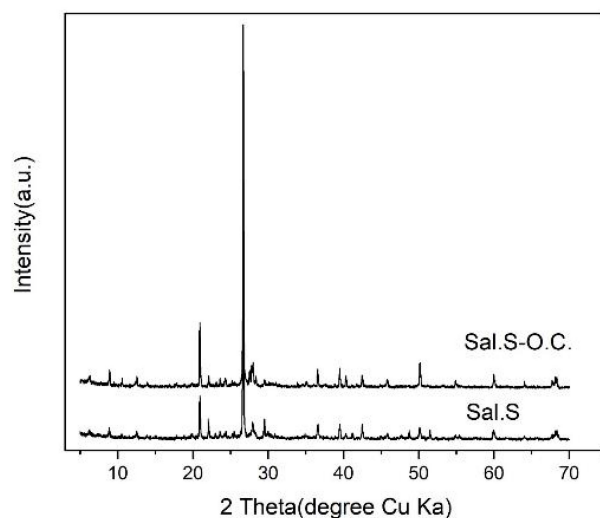


Figure 2. XRD patterns of SASs (Sal.S.) and organic-free SAS (Sal.S.-O.C.).

3.3. Adsorption Isotherms for Cu by Saline–Alkali Soils and Biogas Residue

The Langmuir equation is often used to evaluate the adsorption of adsorbents on a single layer on a polyphase surface [22]. The parameters obtained by the Langmuir model fitting can judge the degree of difficulty of the reaction and the adsorption type [23]. A Langmuir adsorption model was used to fit the adsorption data at 25 °C (Figure 3). The related parameters were shown in Table S2. With the increase in Cu concentration, the adsorption capacity of SAS and BR to Cu increases continuously and finally reaches the adsorption equilibrium. This is mainly because there are a certain number of effective adsorption sites between SAS and BR. When the concentration of Cu is low, enough active adsorption sites can be supplied. However, when the concentration of Cu is high, the amount of Cu is much higher than the number of active groups, and the adsorption of Cu finally reaches saturation. The b values fitted by the Langmuir model are all positive, indicating that the adsorption of Cu by SAS and BR is spontaneous at 25 °C.

Organic substances in soil play an important role in the adsorption of heavy metals [8,24]. After the removal of organic matter, the adsorption capacity of Cu on SASs decreased significantly, and the predicted adsorption capacity Q decreased from 23.21 ± 2.37 mg/g to 0.55 ± 0.017 mg/g. This may be caused by the loss of a large number of effective adsorption active groups in SASs due to the removal of organic matter [25], indicating that the presence of organic matter in SASs has an effect on the adsorption capacity of Cu on SASs. The predicted adsorption capacity Q of BR is obviously higher than that of SAS. It may be that BR contains more active groups than SAS [26], thus providing more active adsorption sites for Cu.

3.4. FTIR Analysis for Saline–Alkali Soil

In recent years, FTIR has been proved to be an effective way to analyse the chemical composition of organic matter [27–29]. Functional groups in the soil, such as carboxyl, hydroxyl, amine and amide, play key roles in the adsorption of heavy metals [30,31]. The FTIR spectra of SASs in Figure 4 shows that the main absorption peaks were 3623, 3536, 3435, 3307, 2873, 2519, 1735, 1676, 1625, 1433, 1336, 1032 and 694 cm^{-1} . The characteristic absorption peaks of alcohols or phenols are sharp absorption peaks at 3623 cm^{-1} in the high frequency region, indicating the stretching vibration of free hydroxyl O–H. The stretching vibration of hydrogen bonds O–H at 3307 cm^{-1} was in the high frequency region. The C–O stretching vibration was at 1032 cm^{-1} , and the out-of-plane bending vibration of O–H was at 694 cm^{-1} . The characteristic absorption peaks of carboxylic acid were at 2873 cm^{-1} and 2519 cm^{-1} ; the broad and strong absorption peaks were O–H stretching vibration absorption. The 1735 cm^{-1} absorption peak was C=O absorption, and the 1336 cm^{-1} absorption peak was C–O stretching vibration absorption. The characteristic

absorption peaks of amides were N–H stretching vibration at 3435 cm^{-1} , C=O stretching vibration at 1676 cm^{-1} , N–H bending vibration at 1625 cm^{-1} and C–N stretching vibration at 1433 cm^{-1} . The characteristic absorption peaks of amines were stretching vibration of N–H at 3435 cm^{-1} , stretching vibration absorption of C–N at 1336 cm^{-1} and 1032 cm^{-1} , formation vibration or scissoring vibration of N–H at 1625 cm^{-1} and out-of-plane bending vibration of N–H at 694 cm^{-1} . Peaks at 3536 cm^{-1} and 1676 cm^{-1} were characteristic for the stretching vibration absorption of unsaturated carbon bonds of olefins.

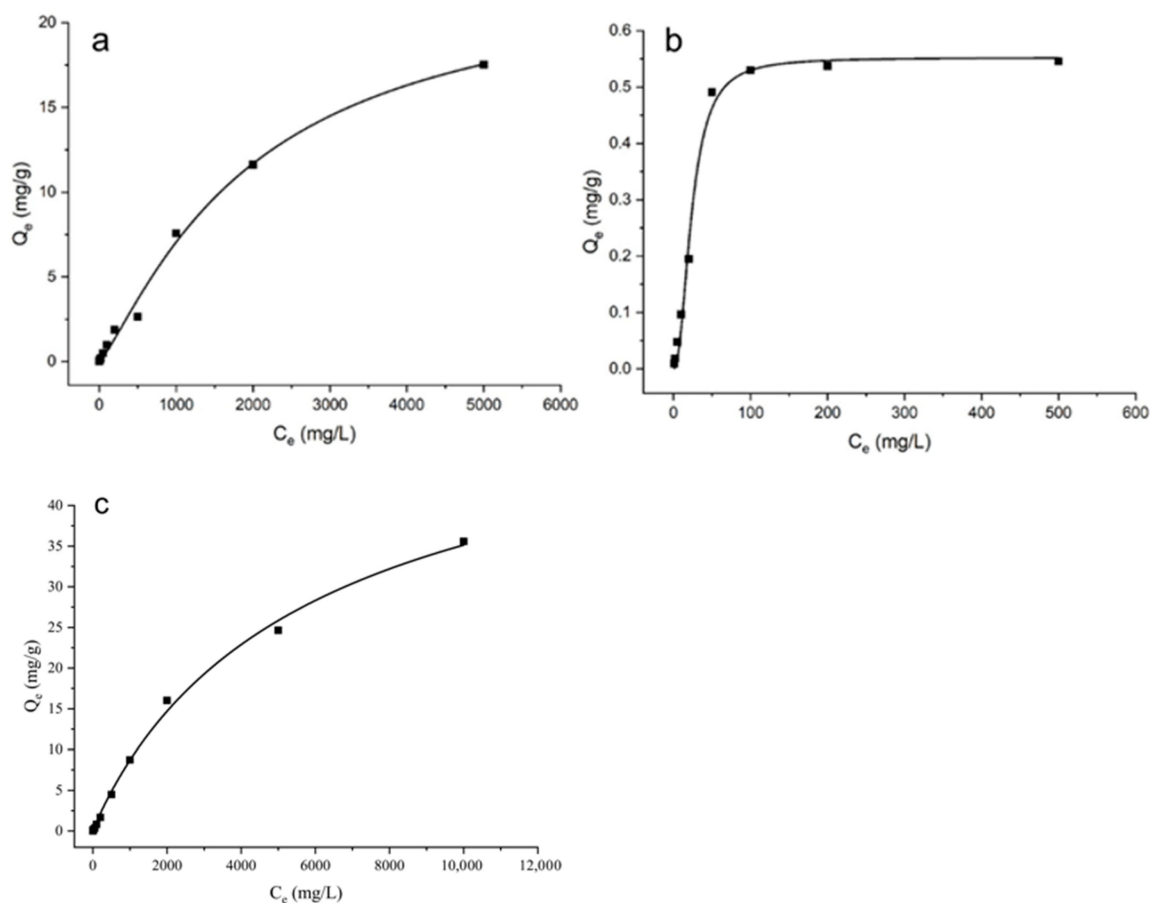


Figure 3. Adsorption isotherms for Cu by SASs (a), remove organic matter (b) and BR (c).

After the removal of organic matter from SASs, the O–H stretching vibration of hydrogen bond between alcohol and phenol molecules at 3307 cm^{-1} , the O–H stretching absorption of carboxylic acid at 2519 cm^{-1} , the C=O absorption of carboxylic acid at 1735 cm^{-1} and the C–N stretching absorption intensity of amide at 1433 cm^{-1} all disappeared or weakened. The stretching vibration of 3623 cm^{-1} alcohol and phenol free hydroxyl O–H, 2873 cm^{-1} carboxylic acid O–H stretching absorption, 2519 cm^{-1} carboxylic acid O–H stretching absorption, 1735 cm^{-1} carboxylic acid C=O absorption, 1433 cm^{-1} amide C–N stretching, 1032 cm^{-1} alcohol and phenol C–O stretching vibration absorption and amine C–N stretching vibration absorption, as well as the 694 cm^{-1} alcohol and phenol O–H and amine N–H out-of-plane bending vibration absorption peaks moved to the high frequency region and became weaker after the adsorption of Cu by saline–alkaline soil. The stretching vibration absorption of 3536 cm^{-1} olefins unsaturated carbon bonds, 3435 cm^{-1} amine N–H stretching vibration, 3307 cm^{-1} alcohol and phenol intermolecular hydrogen bond O–H stretching vibration, 1676 cm^{-1} amide C=O stretching vibration, 1625 cm^{-1} amide and amine N–H bending vibration, 1336 cm^{-1} carboxylic acid C–O stretching and amine C–N stretching vibration absorption strengths became stronger.

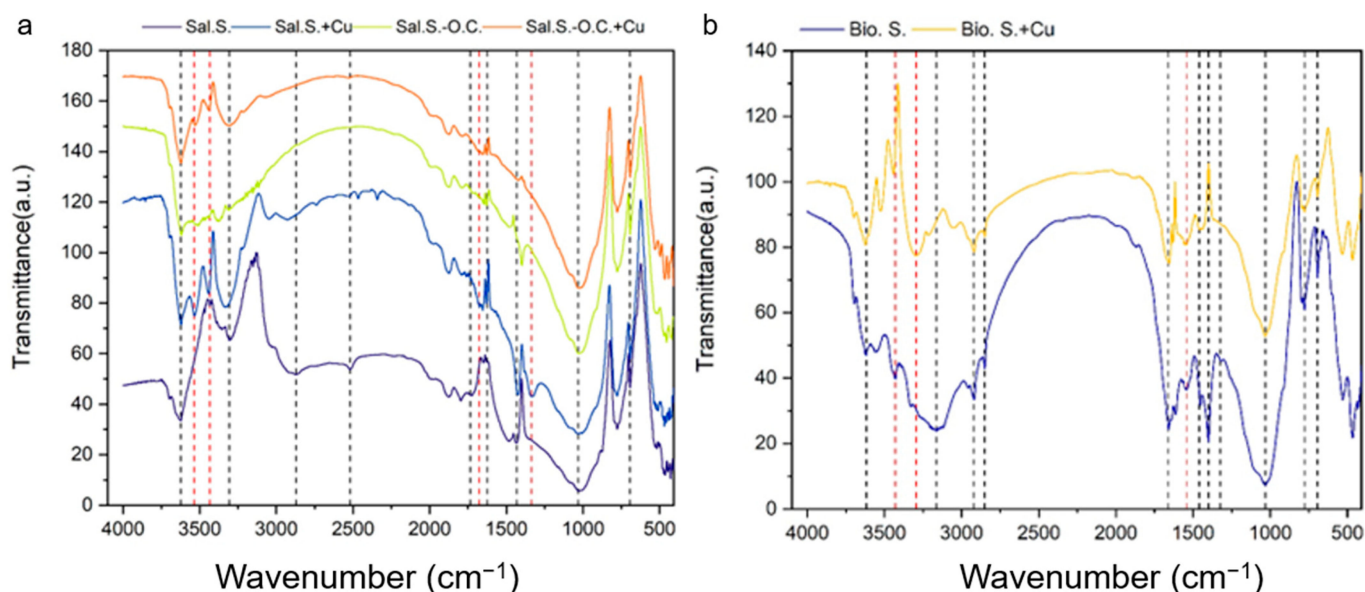


Figure 4. (a): The FTIR spectrums of SASs (Sal.S.) and adsorption Cu (Sal.S. + Cu), remove organic matter (Sal.S.-O.C.) and adsorption Cu (Sal.S.-O.C. + Cu); (b): BR (Bio.S.) and adsorption Cu (Bio.S. + Cu).

In Figure 4, the main absorption peaks of BR are 3619, 3429, 3296, 3162, 2920, 2851, 1659, 1544, 1460, 1401, 1325, 1032, 778 and 694 cm^{-1} . The characteristic absorption peaks of alcohols and phenols are sharp absorption peaks at 3619 cm^{-1} in the high frequency region, with the stretching vibration of free hydroxyl O–H and the stretching vibration of hydrogen bond O–H at 3296 cm^{-1} in high frequency region as well as the stretching vibration of C–O at 1032 cm^{-1} and the out-of-plane bending vibration of O–H at 694 cm^{-1} . The characteristic absorption peaks of carboxylic acid are the broad and strong absorption peaks of 3162 cm^{-1} are O–H stretching absorption, and the absorption peaks of 1325 cm^{-1} are C–O stretching absorption. The characteristic absorption peaks of amide are the N–H stretching vibration at 3429 cm^{-1} , C=O stretching vibration at 1659 cm^{-1} and the C–N stretching vibration at 1401 cm^{-1} . The characteristic absorption peaks of amines are a stretching vibration of N–H at 3429 cm^{-1} , stretching vibration absorption of C–N at 1325 cm^{-1} , formation vibration or scissoring vibration of N–H at 1544 cm^{-1} and an out-of-plane bending vibration of N–H at 694 cm^{-1} . The peak at 778 cm^{-1} is an aliphatic organic halide C–X stretching vibration. The 2920 cm^{-1} , 2850 cm^{-1} and 1460 cm^{-1} peaks are the stretching vibration absorption peaks of aliphatic methylene. The absorption peaks of alcohol and phenol free hydroxyl O–H at 3619 cm^{-1} , amide or amine N–H at 3429 cm^{-1} , amide C=O at 1659 cm^{-1} and amine N–H at 1544 cm^{-1} all increased after the adsorption of Cu by BR. The absorption peaks of carboxylic acid O–H stretching absorption at 3162 cm^{-1} , amide C–N stretching at 1401 cm^{-1} , carboxylic acid C–O or amine C–N stretching at 1325 cm^{-1} , aliphatic organic halides C–X stretching at 778 cm^{-1} , and alcohol and phenol O–H and amine N–H out-of-plane bending vibration 694 cm^{-1} absorption peaks were weakened after adsorption of Cu. This is consistent with previous studies on Cu adsorption [32–36].

3.5. Thermodynamic Analysis

With the development of ITC technology, it has been successfully applied in many theories and practices in the field of environment [37–39]. Complete thermodynamic parameters such as reaction stoichiometry (n), binding constant (K), enthalpy change (ΔH) and entropy change (ΔS) can be obtained by ITC fitting. Figure 5 is isothermal titration data of Cu^{2+} in a single system. The thermodynamic parameters are fitted by the unit point independent model (Table S3). The adsorption of carboxyl ($-\text{COOH}$) to Cu is an enthalpy-decreasing process, an exothermic reaction ($\Delta H = -3.62 \text{ kJ/mol}$), and

the adsorption of amino ($-\text{NH}_2$) to Cu is an enthalpy-increasing process, an endothermic reaction ($\Delta H = 216 \text{ kJ/mol}$). Table S3 shows that the entropy (ΔS) of Cu on the surface of carboxyl and amino groups of the adsorbent is positive, and the adsorption is a process of increasing disorder, which may be due to the formation of complexes between Cu^{2+} and functional groups on the surface of the adsorbent, resulting in atomic rearrangement. According to the thermodynamic binding parameter K value, the affinity of carboxyl group on the surface of adsorbent to Cu is higher than that of amino group. By comparing the absolute value $|\Delta H|$ and $|\Delta S|$, the driving force of Cu adsorption on the adsorbent surface can be preliminarily judged. The adsorption of Cu on adsorbent carboxyl group $|\Delta H| < |\Delta S|$ and $\Delta H < 0$, indicating that entropy and enthalpy were controlled [40,41]; however, the adsorption of Cu on adsorbent amine group $|\Delta H| > |\Delta S|$ and $\Delta H > 0$, indicating that it is driven by entropy [37,42]. The adsorption of Cu on the carboxyl group of the adsorbent $\Delta G < 0$ indicates that the reaction can proceed spontaneously at 25°C without external energy supply for the reaction system. The adsorption of Cu on the amine group of the adsorbent $\Delta G > 0$ indicates that the reaction cannot proceed spontaneously at 25°C and requires an external energy supply for the reaction system to drive the reaction.

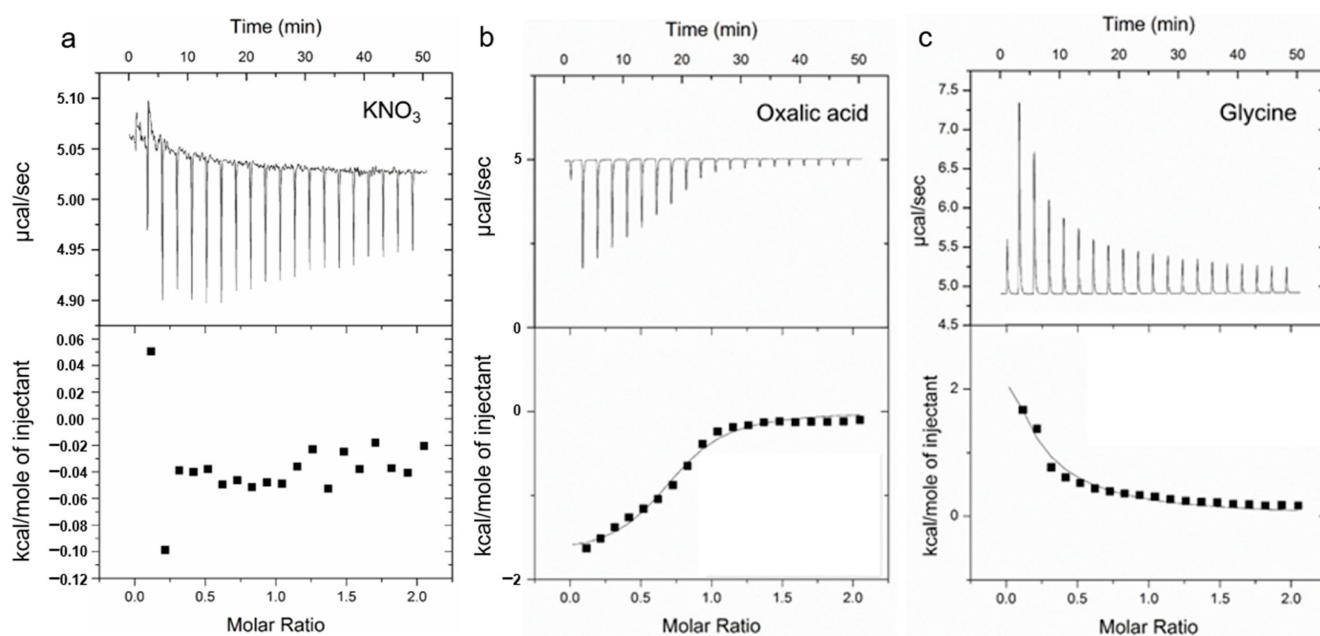


Figure 5. Isothermal titration data for the addition of Cu(II) to oxalic acid (carboxyl) (b), glycine (amino) (c) in 1 mol/L KNO_3 background electrolyte (pH 5) at 25°C (a). The upper and lower panels of each graph represent calorimetric titrations (heat flow) and integrated heat values, respectively. The solid line represents the best independent model fitting results.

3.6. XPS Analysis of Biogas Residue and Saline–Alkali Soil

XPS is a surface analysis method that can give important information about the kinds of elements, chemical composition and related electronic structures on the surface of solid samples [43–45]. XPS can clarify the chemical state of atoms bound with Cu ions in soil [46–49]. In Figure 6, the survey scans of SAS contained O, C, Si, Ca, Al and Mg. The survey scans did not show the presence of Cu. The XPS survey scan of Cu adsorption on SASs contains O, C, Si, Ca, Al, Mg and Cu. The existence of Cu in the survey scan shows that Cu has been combined with SASs. The XPS analysis of SASs before and after Cu adsorption showed that the characteristic peaks of $\text{Cu } 2p_{1/2}$ and $2p_{3/2}$ appeared in the survey scan of SASs after Cu adsorption. Figure 6 shows that the binding energy of C 1s, Cu 2p and O 1s all change after the removal of organic matter from SAS, and the adsorption of Cu by samples, indicating that the chemical environment of the elements in the sample has changed significantly.

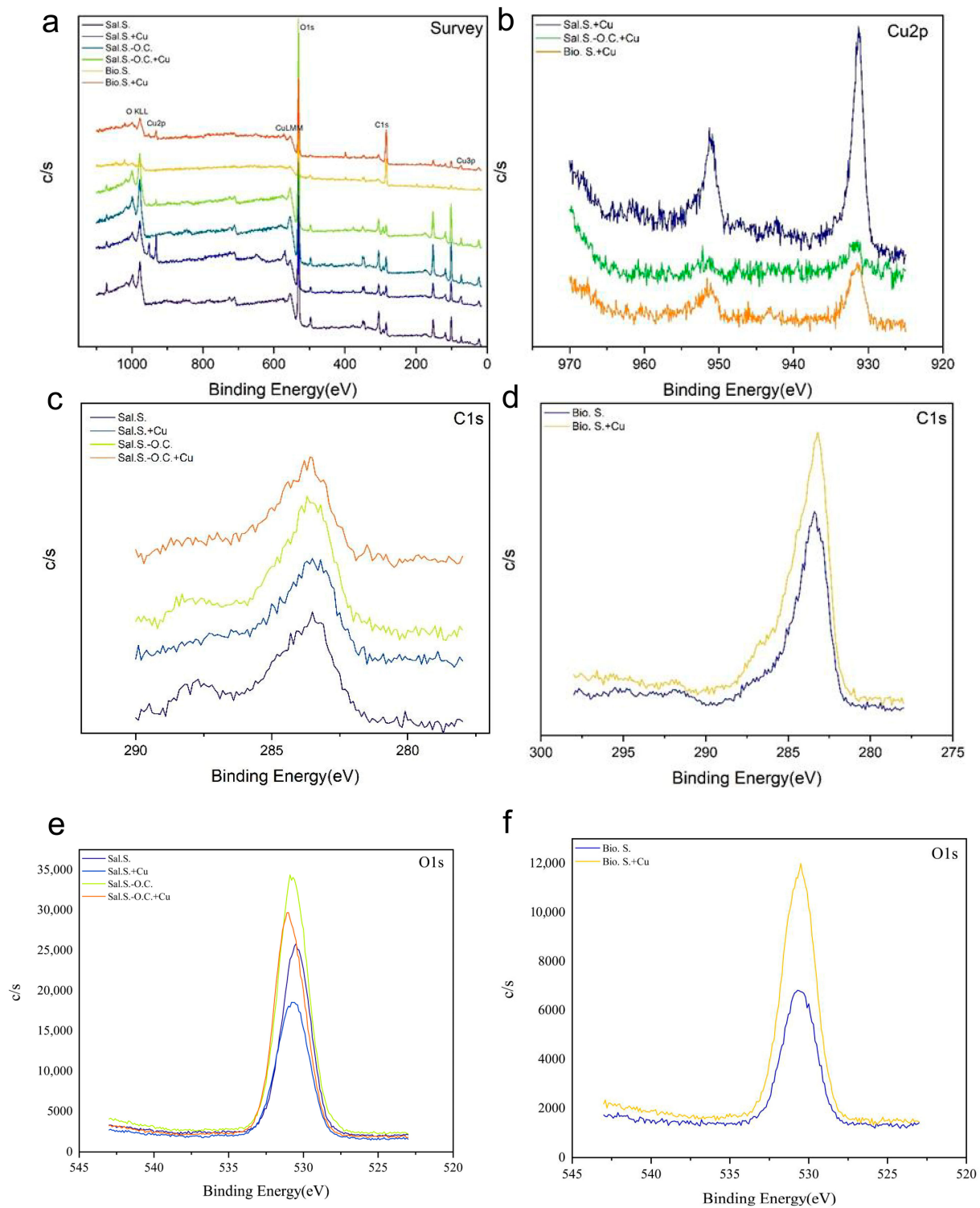


Figure 6. The XPS spectra of saline–alkali soils (Sal.S.) (a) and adsorption Cu (Sal.S. + Cu) (b), remove organic matter (Sal.S.-O.C.) (c) and adsorption Cu after removing organic matter (Sal.S.-O.C. + Cu) (e), biogas residue (Bio.S.) (d) and adsorption Cu (Bio.S. + Cu) (f).

C 1s can be fitted to C–C, C–O and O=C–O by high-resolution scanning peak analysis of C in SAS (Figure 7). After removing organic matter from SAS, C 1s can be fitted to C–C, C–O and C–H. Through analysis (Table S4), it was found that C–C did not change significantly, C–O decreased significantly, O=C–O disappeared and C=O and C–H appeared. The change of functional groups in SAS after removal of organic matter was confirmed.

Comparing with the peak analysis of C elements before and after the adsorption of Cu by SAS (Figure 7), the C 1s of SAS can be fitted as C–C, C–O and C=O. After the adsorption of Cu by SAS, C–O decreased obviously, O=C–O disappeared, and C=O appeared, which may be because the binding of Cu with hydroxyl and carboxyl groups in the process of adsorption on SASs results in the change of group electron cloud. High resolution scanning peak analysis of C element before and after the removal of organic matter from SAS (Figure 7) showed that C 1s after the removal of Cu could be fitted to C–C, C–O, C=O and C–H, and the relative areas of peaks changed (Table S4). After the removal of organic matter from SAS, C–C decreased significantly and C=O increased significantly, and the hydroxyl and carboxyl group were lost, but the remaining functional groups still had the ability to adsorb Cu, although the ability to adsorb Cu decreased significantly (Figure 3, Table S2). After adsorption of Cu with SASs, the high-resolution scanning peak analysis of Cu in SASs (Figure 7, Table S4) shows that the peak of Cu 2p could be fitted to two chemical valence states of Cu(I) and Cu(II). After the removal of organic matter from SASs, the peak areas of Cu(I) and Cu(II) decreased significantly, which is in comparison with those in SASs. The decrease in active functional groups is related to the adsorption of Cu in SASs, and the peak area of Cu(II) was slightly larger than that of Cu(I). After removing organic matter from SASs, the peak area of Cu(II) was much higher than that of Cu(I), indicating that the adsorption of Cu in SASs is accompanied by redox [10,50]. At the same time, the peak position of O 1s was detected to change (Figure 6), indicating that the adsorption of Cu by SASs may be supplied by the O atoms of carboxyl and hydroxyl groups.

The C 1s peak can be fitted to C–C, C–O, C–N and –COOH by analysing the high-resolution scanning map of C in BR (Figure 8). The C 1s peak can be fitted to C–C, C–O, C–N and C=O after adsorption of Cu by BR. It was found that C–O and C–C obviously increased, –COOH disappeared and C=O occurred after adsorption of Cu (Table S5), indicating that the adsorption of Cu results in the change of the electron cloud of functional groups. After the adsorption of Cu by BR (Figure 8), the peak of Cu 2p could be fitted to two chemical valence states of Cu(I) and Cu(II). The peak area of Cu(II) in BR was much higher than that of Cu(I). It shows that the adsorption of Cu in BR was accompanied by redox. Complexation reactions took precedence over redox reactions. The disappearance of –COOH may be due to the complexation of Cu, and the increase in C–O and C–C binding energy may be due to the participation in the redox of Cu [51–53].

3.7. SEM–EDS Analysis of Distribution of Cu in Alkali Soil and Biogas Residue

The morphology of materials can be obtained by SEM, and the distribution of elements on the surface of materials can be analysed by EDS. Figure 9 shows the SEM–EDS spectrum of SAS after adsorption of Cu. The uniform distribution of O, Al and Si elements on the surface of SASs indicates that the main mineral of SASs is aluminosilicate, and it contains K, Ca and Fe, which is consistent with the results of mineral identification of SASs by XRD (Figure 2, Table S1). C may represent the granular distribution of carbonate minerals (e.g., calcite, Table S1) on the surface of SASs, while P represents the independent mineralisation of phosphorus-bearing minerals (e.g., struvite, Table S1) and their combination on the surface of SASs. Cu elements are uniformly distributed on the surface of saline–alkali soil but concentrate on a specific mineral on the surface of the main mineral. Through EDS point scanning analysis of three specific mineral sites of Cu element distribution, it is concluded that all three specific sites contained O, Si, C, Cu, Mg, Al, Fe and Ca (Table S6, arranged from large to small according to normalised mass percentage). Cu may bind to organic matter on SAS surfaces [11,54].

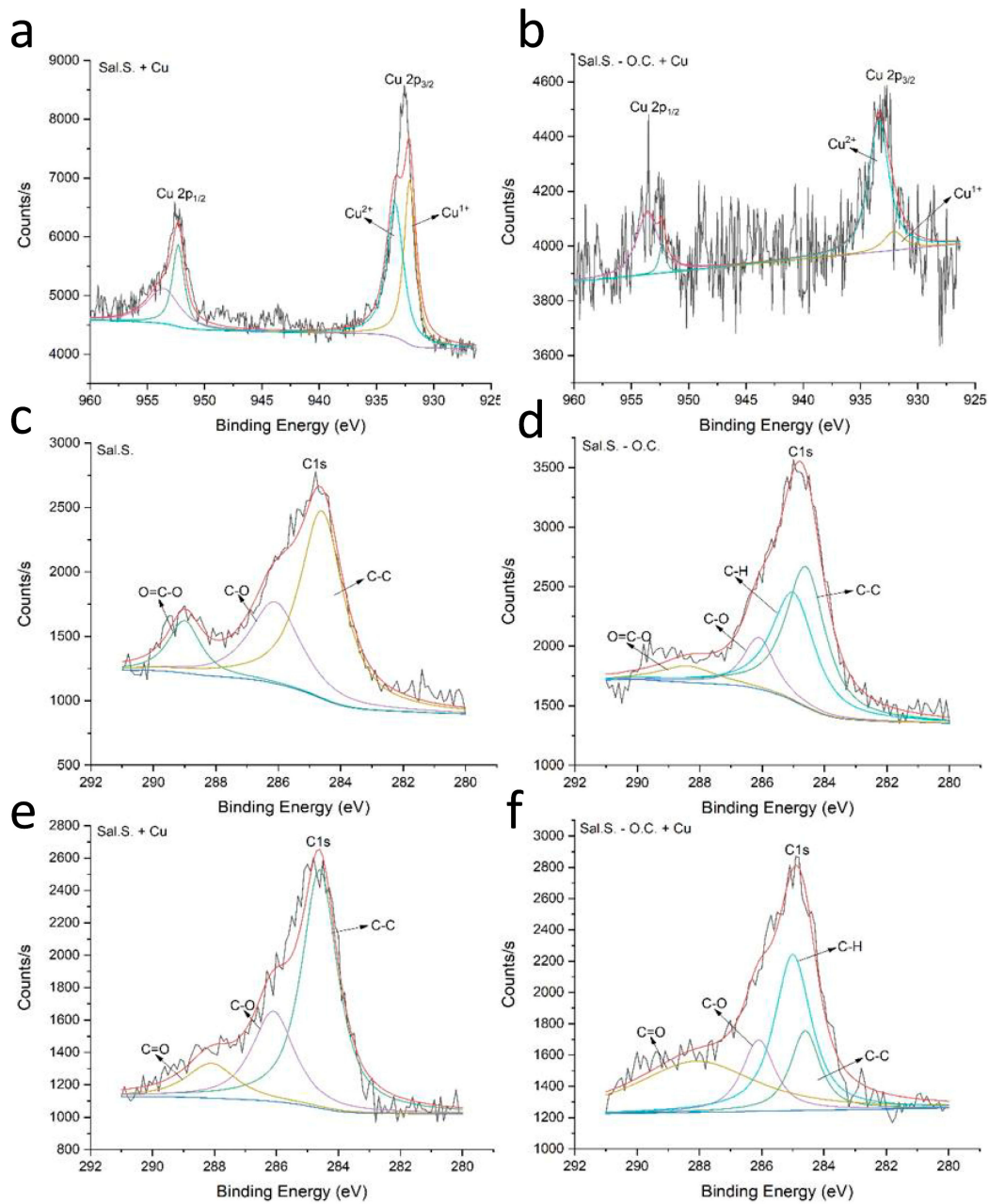


Figure 7. The XPS spectra of C 1s and Cu 2p (a,b) from the surface of SASs (Sal.S.) (c) and adsorption Cu (Sal.S. + Cu) (d), remove organic matter (Sal.S.-O.C.) (e) and adsorption Cu after removing organic matter (Sal.S.-O.C. + Cu) (f).

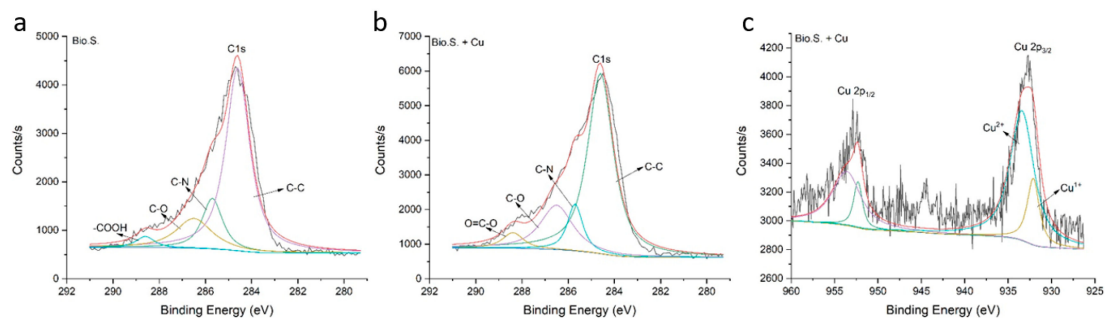


Figure 8. The XPS spectra of C 1s and Cu 2p (c) from the surface of BR (Bio.S.) (a) and adsorption Cu (Bio.S. + Cu) (b).

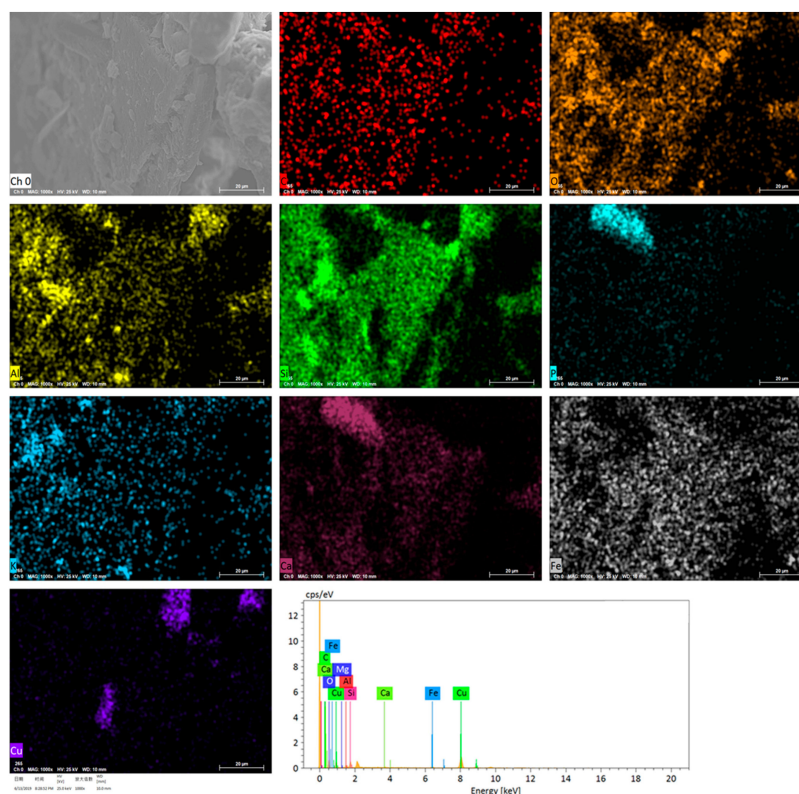


Figure 9. SEM image and the corresponding EDS mapping of SASs after adsorption Cu.

Figure 10 is the SEM–EDS spectrum of the adsorption of Cu by BR. C, O and P on the surface of BR are uniformly distributed, and contain K, Ca, Fe and Zn. It shows that BR is an organic matter containing nutrient elements P, K, Ca, Fe and Zn. The distribution of Al and Si indicates that the minerals containing Al and Si on the surface of BR are granular, and the existence of minerals may be due to the minerals contained in the sewage sludge, which was the inoculant of biogas digestion. The uniform distribution of Cu on the surface of SAS indicates that the adsorption of Cu by BR is accomplished by a large number of active groups [13,55–57]. The minerals indicated by BR do not adsorb Cu, which indicates that the adsorption of Cu in BR was done by organic matter rather than minerals, which is consistent with the results of the adsorption of Cu in SAS (Figure 9) and XPS analysis (Figure 7).

3.8. Analysis of Decomposition Process of Biogas Residue in Saline–Alkali Soil Based on FTIR

In Figure 11, FTIR spectrums of SASs and application of 2% BR are for one, two, three, four and five seasons. The main absorption peaks were 3621, 3524, 3442, 3305, 2519, 1653, 1629, 1429, 1031, 778 and 694 cm^{-1} . The characteristic absorption peaks of alcohols and phenols are sharp absorption peaks at 3621 cm^{-1} in the high frequency region; stretching vibration of free hydroxyl O–H of alcohols and phenols; stretching vibration of hydrogen bond O–H between alcohols and phenols at 3305 cm^{-1} in the high frequency region; stretching vibration of alcohol and phenol C–O at 1031 cm^{-1} ; and out-of-plane bending vibration of alcohol and phenol C–O at 694 cm^{-1} . The characteristic absorption peaks of amides are the amide N–H stretching vibration at 3524 cm^{-1} in the high frequency region; the amide C=O stretching vibration at 1653 cm^{-1} ; the amide N–H bending vibration at 1629 cm^{-1} ; and the amide C–N stretching vibration at 1429 cm^{-1} . The characteristic absorption peaks of amines are the stretching vibration of amine N–H at 3442 cm^{-1} ; the stretching vibration of amine C–N at 1031 cm^{-1} ; the formation vibration or scissoring vibration of amine N–H at 1629 cm^{-1} ; and out-of-plane bending vibration of amine N–H at 778 cm^{-1} . The absorption peak of 2519 cm^{-1} may be O–H stretching absorption of carboxylic acid.

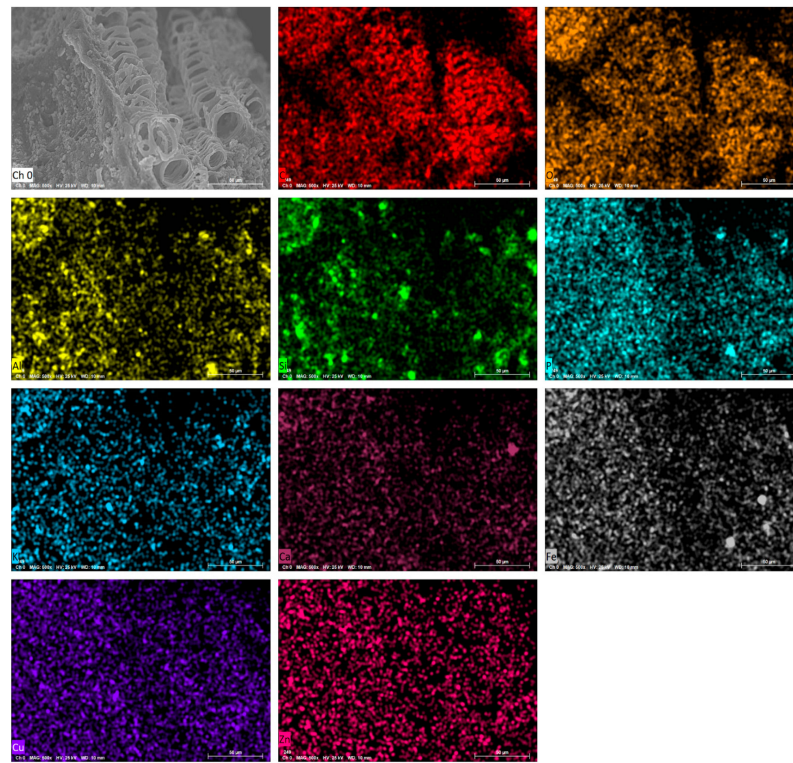


Figure 10. SEM image and the corresponding EDS mapping of BR after adsorption Cu.

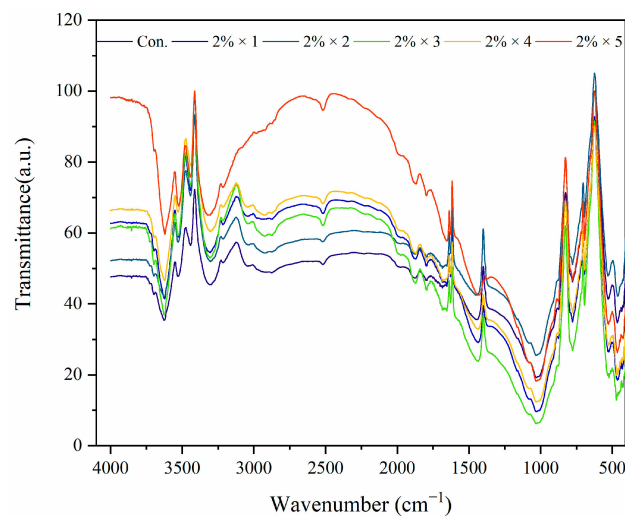


Figure 11. The FTIR spectrums of SASs (Con.) and application of 2% BR for one season ($2\% \times 1$), two seasons ($2\% \times 2$), three seasons ($2\% \times 3$), four seasons ($2\% \times 4$), five seasons ($2\% \times 5$).

By comparing the FTIR spectra of different BR application modes, the infrared spectra of different application modes are similar, which shows that the SAS with different application modes of Cu-rich marsh residue has the same structure. However, the peak position and intensity of some characteristic peaks changed. From the overall characteristics, the continuous application of Cu-rich BR in SAS increased, the main absorption peak intensity gradually increased, and the peak position gradually “red shift”. N–H formation vibration or scissoring vibration, C=O stretching vibration and C–N stretching vibration of amides and amines represent proteins in SAS. The stretching vibration of free hydroxyl O–H, O–H stretching vibration of the intermolecular hydrogen bond and O–H out-of-plane bending represent polysaccharides and cellulose in SAS. Table S7 shows that the strength of the main absorption peaks increases when the Cu-rich BR is continuously applied for five

seasons, compared with the non-application, indicating that the application of BR increases the content of protein, polysaccharide and cellulose in SAS.

The intensity of absorption peaks in SAS treated with BR for one season decreased in varying degrees compared with that applied for five growing seasons. This indicates that the BR applied to SAS was continuously decomposed and utilised by soil microorganisms during the five-season crop planting process, and the contents of protein, polysaccharide and cellulose were continuously reduced. Compared with that without Cu-rich BR, the strength of the main absorption peaks of polysaccharide and cellulose (3621 cm^{-1} and 3305 cm^{-1}) were still higher than that of the control, and the strength of main absorption peaks of protein 1653 , 1031 , 1629 , 1430 and 778 cm^{-1} were close to or lower than that of the control. The results showed that the polysaccharide and cellulose components of 2% Cu-rich BR applied in SAS had not been completely degraded, but the protein components had been completely degraded after five seasons of crop cultivation and soil microbial decomposition. The main absorption peak intensity was the lowest in three consecutive seasons. This may be due to decomposition of BR in SAS after three consecutive seasons, which resulted in the highest soil microbial activity. The application of Cu-rich BR for three growing seasons also ensured the maintenance of soil microbial activity.

3.9. Behaviour of Cu in Saline–Alkali Soil after Application of Biogas Residue Based on XPS Analysis

In order to analyse the migration of Cu during the application of BR in SAS, the chemical environment of Cu adsorbed on SAS was characterised by XPS. The specific adsorption of Cu in SAS was explored by measuring the characteristics and relative content of surface elements. Figure 12 shows the survey spectra of C 1s, O 1s, N 1s, Cu 2s, Cu 2p, Cu 3s and Cu 3p in SAS after applying BR. It describes the change of binding energy of different ways of applying BR in SAS. It can be seen from Figure 12 that there are similar peaks, indicating that SAS contains similar elements after applying different ways. Because the binding energy of Cu 3p and Al 2p is similar, their peaks overlap, and the presence of Cu in SASs is demonstrated in Figure 12. In order to analyse the chemical forms of Cu in SASs, the peaks of Al and Cu were separated. As shown in Figure 13, the occurrence of the peaks of Cu(I) could be clearly seen. By comparing the peak area of the same element, we can know the relative content of the element atom.

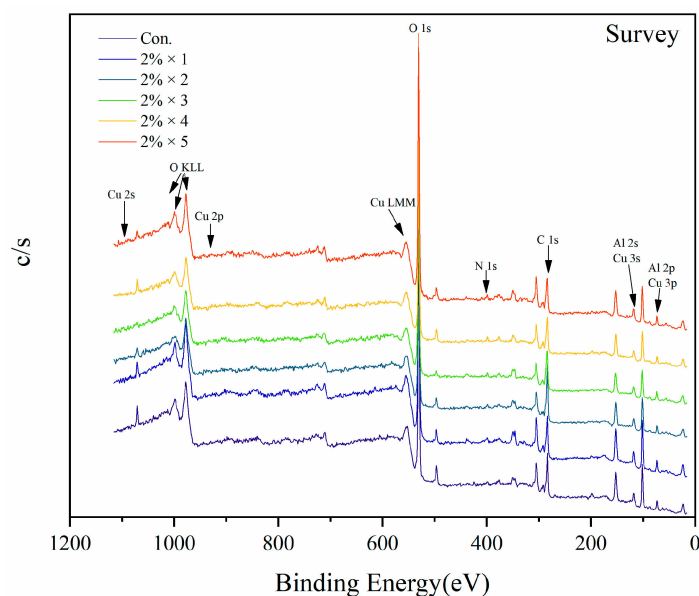


Figure 12. The XPS spectra of saline–alkali soils (Con.) and application of 2% biogas residue for one season ($2\% \times 1$), two seasons ($2\% \times 2$), three seasons ($2\% \times 3$), four seasons ($2\% \times 4$), five seasons ($2\% \times 5$).

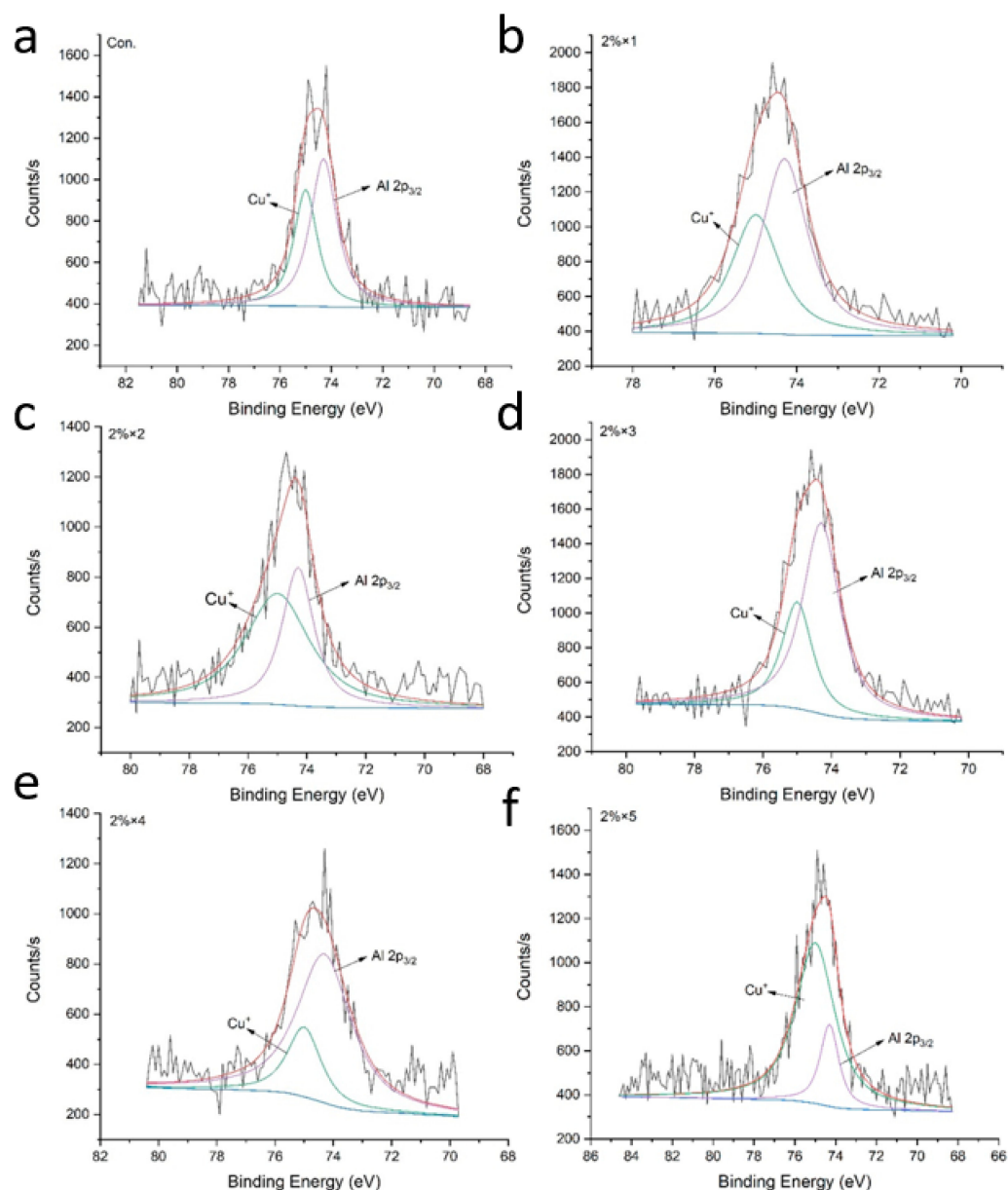


Figure 13. The XPS spectra of Cu 3p from the surface of SASs (Con.) (a), and application of 2% BR for one season ($2\% \times 1$) (b), two seasons ($2\% \times 2$) (c), three seasons ($2\% \times 3$) (d), four seasons ($2\% \times 4$) (e), five seasons ($2\% \times 5$) (f).

In the process of fitting the peaks of Cu 3p, it was found that there were no peaks of Cu(II) and there were peaks of Cu(I) in the BR (Figure 8). This indicated that the Cu(II) in BR was reduced to Cu(I) in the SAS during the application of the BR. Table S8 shows that the area of Cu peak in SAS increased after applying biogas fertiliser.

After fertiliser was applied continuously for five seasons, the area of the Cu peak was the highest. It is speculated that the continuous application of BR cannot significantly change the redox environment of soil, which indicates that SAS has a better potential buffer environment and the ability to absorb BR. With the increase in degradation time of BR in SAS, the area of Cu(I) peak on the surface of SAS first decreases and then increases to the area similar to that on the control surface, then increases and then decreases, which is a fluctuating change. It is speculated that the addition of BR in SAS increases the protein and polysaccharide content in SAS. Free Cu produced by microbial decomposition is preferentially combined with BR when there is continuous decomposition of BR. With the increase in Cu, the redistribution of Cu between SAS and BR is continually increasing, and

the amount of organic matter bound to SAS is also increasing. A portion of Cu enters into the intercalated organic matter of SAS and may enter into SAS minerals (the peak of Cu 3p was also found in the control). The area of Cu 3p peak of 2% × 1 was higher than that of the control, and the content of organic matter in the intercalated organic matter of SAS was 3.67 ± 0.17 g/kg.

3.10. Distribution of Cu in Saline–Alkali Soil after Continuous Application of Biogas Residue Based on Micro-XRF Analysis

Micro-XRF imaging technology can analyse the element composition and two-dimensional distribution of samples in situ, and it can allow the intuitive understanding of the distribution of target elements in complex systems. Five consecutive seasons of BR were applied in SAS. Ca, P and Mg were evenly distributed in SAS, indicating homogeneous mineral types of SAS. The distribution map of Cu in SAS with the large and bright red dots in the concentration of Cu elements intuitively shows the adsorption of Cu in the non-degraded BR during continuous application. Small and fine red dots intuitively present the combined Cu of BR and SAS after degradation. The red dot between them intuitively shows the adsorption of Cu by BR with different degradation degrees. This shows that BR is degraded continuously in SAS, and after degradation, Cu is adsorbed on the surface or inside of SAS (Figure 14).

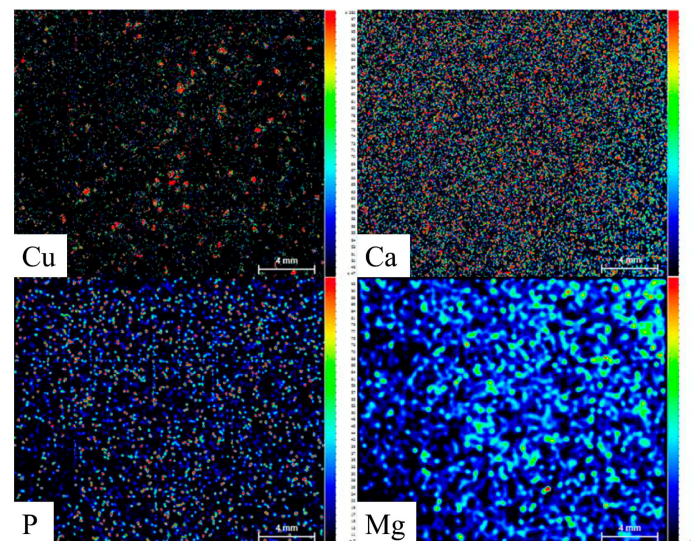


Figure 14. Distribution of Cu, Ca, P, Mg in SASs after application of BR for five seasons under the micro-XRF.

4. Conclusions

In summary, the pH of the SAS decreased and the organic matter content increased after the application of BR, while the Cu content of the SAS did not exceed the limit value of the national standard. After the application of BR, the main groups for Cu adsorption by the SAS and BR were carboxyl, hydroxyl, amide and amine. The adsorption of Cu to the SAS and BR was achieved by organic matter rather than minerals. The degradation of BR in the SAS increases the content of Cu adsorption groups such as carboxyl and amine groups, and Cu is adsorbed on the surface or inside the SAS through organic groups. This study elucidates the mechanism of Cu reversion during SAS application of BR of a Cu-contaminated soil phytoremediation plant (*Elsholtzia splendens*). Therefore, anaerobic fermentation of plant residues is an effective method for the rational use of phytoremediation plants.

Supplementary Materials: The following supporting information can be downloaded at: <https://www.mdpi.com/article/10.3390/agriculture13040915/s1>, S1 Additional descriptions about the experiments. Table S1 The variety and relative amount of saline-alkali soils (Sal.S.) and organic-free saline-alkali soil (Sal.S.-O.C.). Table S2 Fitting parameters for adsorption isotherms of Cu on saline-alkali soil, organic-free saline-alkali soil and biogas residue. Table S3 Thermodynamic parameters for Cu adsorption in oxalic acid and glycine at pH 5 and 25 °C in 1 mol/L KNO₃ electrolyte. Table S4 The area of C 1s and Cu 2p from the surface of saline-alkali soils and adsorption Cu, remove organic matter and adsorption Cu after remove organic matter. Table S5 The area of C 1s and Cu 2p from the surface of biogas residue and adsorption Cu. Table S6 The percentage of SEM-EDS of saline-alkali soils after adsorption Cu. Table S7 Relative intensity of major absorption packs in saline-alkali soils (Con.) and application of 2% biogas residue for one season (2% × 1), two seasons (2% × 2), three seasons (2% × 3), four seasons (2% × 4), five seasons (2% × 5). Table S8 The area of Cu 3p from the surface of saline-alkali soils (Con.) and application of 2% biogas residue for one season (2% × 1), two seasons (2% × 2), three seasons (2% × 3), four seasons (2% × 4), five seasons (2% × 5). Table S9 Total organic carbon content in saline-alkali soil, organic-free SAS and biogas residue.

Author Contributions: Conceptualization, B.L. and S.W.; data curation, B.L. and S.W.; formal analysis, P.D.; funding acquisition, L.S. and Y.C.; investigation, L.Z. and L.S.; methodology, B.L.; project administration, Z.S.; resources, X.Z.; software, S.W. and Y.X.; supervision, X.X.; validation, B.L.; writing—review and editing, C.C., L.S. and Y.C. All authors have read and agreed to the published version of the manuscript.

Funding: This study was supported by the Scientific and Technological Innovation Fund of Carbon Emissions Peak and Neutrality of Jiangsu Provincial Department of Science and Technology (BE2022304), the earmarked fund for CARS-10-Sweetpotato, the National Key R&D Program of China (2021YFC1809100), the National Natural Science Foundation of China (31901180; 41571307).

Institutional Review Board Statement: Not applicable.

Data Availability Statement: No sharing of research data due to privacy.

Conflicts of Interest: The authors declare no conflict of interest.

References

- Lombi, E.; Susini, J. Synchrotron-based techniques for plant and soil science: Opportunities, challenges and future perspectives. *Plant Soil* **2009**, *320*, 1–35. [[CrossRef](#)]
- Papuga, K.; Kaszubkiewicz, J.; Kawalko, D.; Kreimeyer, M. Effect of Organic Matter Removal by Hydrogen Peroxide on the Determination of Soil Particle Size Distribution Using the Dynamometer Method. *Agriculture* **2022**, *12*, 226. [[CrossRef](#)]
- Ippolito, J.A.; Barbarick, K.A.; Brobst, R.B. Copper and Zinc speciation in a biosolids-amended, semiarid grassland soil. *J. Environ. Qual.* **2014**, *43*, 1576–1584. [[CrossRef](#)] [[PubMed](#)]
- Tella, M.; Bravin, M.N.; Thuries, L.; Cazevieille, P.; Chevassus-Rosset, C.; Collin, B.; Chaurand, P.; Legros, S.; Doelsch, E. Increased zinc and copper availability in organic waste amended soil potentially involving distinct release mechanisms. *Environ. Pollut.* **2016**, *212*, 299–306. [[CrossRef](#)] [[PubMed](#)]
- Mondaca, P.; Neaman, A.; Sauve, S.; Salgado, E.; Bravo, M. Solubility, partitioning, and activity of copper-contaminated soils in a semiarid region. *J. Plant Nutr. Soil Sci.* **2015**, *178*, 452–459. [[CrossRef](#)]
- Mamindy-Pajany, Y.; Sayen, S.; Mosselmans, J.F.W.; Guillon, E. Copper, Nickel and Zinc speciation in a biosolid-amended soil: pH adsorption edge, mu-XRF and mu-XANES investigations. *Environ. Sci. Technol.* **2014**, *48*, 7237–7244. [[CrossRef](#)]
- Sarker, T.C.; Incerti, G.; Spaccini, R.; Piccolo, A.; Mazzoleni, S.; Bonanomi, G. Linking organic matter chemistry with soil aggregate stability: Insight from C-13 NMR spectroscopy. *Soil Biol. Biochem.* **2018**, *117*, 175–184. [[CrossRef](#)]
- Liu, L.; Guo, X.; Zhang, C.; Luo, C.; Xiao, C.; Li, R. Adsorption behaviours and mechanisms of heavy metal ions' impact on municipal waste composts with different degree of maturity. *Environ. Technol.* **2018**, *40*, 2962–2976. [[CrossRef](#)]
- Lockwood, C.L.; Stewart, D.I.; Mortimer, R.J.G.; Mayes, W.M.; Jarvis, A.P.; Gruiz, K.; Burke, I.T. Leaching of copper and nickel in soil-water systems contaminated by bauxite residue (red mud) from Ajka, Hungary: The importance of soil organic matter. *Environ. Sci. Pollut. Res.* **2015**, *22*, 10800–10810. [[CrossRef](#)]
- Fulda, B.; Voegelin, A.; Maurer, F.; Christl, I.; Kretzschmar, R. Copper redox transformation and complexation by reduced and oxidized soil humic acid. 1. X-ray absorption spectroscopy study. *Environ. Sci. Technol.* **2013**, *47*, 10903–10911. [[CrossRef](#)]
- Maurer, F.; Christl, I.; Fulda, B.; Voegelin, A.; Kretzschmar, R. Copper redox transformation and complexation by reduced and oxidized soil humic acid. 2. potentiometric titrations and dialysis cell experiments. *Environ. Sci. Technol.* **2013**, *47*, 10912–10921. [[CrossRef](#)] [[PubMed](#)]

12. Wang, S.; Zhang, L.; Jiang, M.; Wang, J.; Xia, F.; Shi, L.; Xia, Y.; Chen, C.; Shen, Z.; Chen, Y. Cyclic and safety utilisation of Cu polluted biogas residue in saline-alkali soil. *Sci. Total Environ.* **2020**, *704*, 135410. [[CrossRef](#)]
13. Graouer-Bacart, M.; Sayen, S.; Guillon, E. Macroscopic and molecular approaches of enrofloxacin retention in soils in presence of Cu(II). *J. Colloid Interface Sci.* **2013**, *408*, 191–199. [[CrossRef](#)] [[PubMed](#)]
14. Zachara, J.M.; Smith, S.C.; Resch, C.T.; Cowan, C.E. Cadmium sorption to soil separates containing layer silicates and iron and aluminum-oxides. *Soil Sci. Soc. Am. J.* **1992**, *56*, 1074–1084. [[CrossRef](#)]
15. Kahle, M.; Kleber, M.; Jahn, R. Predicting carbon content in illitic clay fractions from surface area, cation exchange capacity and dithionite-extractable iron. *Eur. J. Soil Sci.* **2002**, *53*, 639–644. [[CrossRef](#)]
16. Rahman, M.M.; Liu, Y.; Kwag, J.; Ra, C. Recovery of struvite from animal wastewater and its nutrient leaching loss in soil. *J. Hazard. Mater.* **2011**, *186*, 2026–2030. [[CrossRef](#)] [[PubMed](#)]
17. Wang, H.; Wang, X.; Wang, W.; Yan, X.; Xia, P.; Chen, J.; Zhao, J. Modeling and optimization of struvite recovery from wastewater and reusing for heavy metals immobilization in contaminated soil. *J. Chem. Technol. Biotechnol.* **2016**, *91*, 3045–3052. [[CrossRef](#)]
18. De Godoi, F.C.; Rodriguez-Castellon, E.; Guibal, E.; Beppu, M.M. An XPS study of chromate and vanadate sorption mechanism by chitosan membrane containing copper nanoparticles. *Chem. Eng. J.* **2013**, *234*, 423–429. [[CrossRef](#)]
19. Matjie, R.H.; French, D.; Ward, C.R.; Pistorius, P.C.; Li, Z. Behaviour of coal mineral matter in sintering and slagging of ash during the gasification process. *Fuel Process. Technol.* **2011**, *92*, 1426–1433. [[CrossRef](#)]
20. Ouhadi, V.R.; Yong, R.N.; Rafiee, F.; Goodarzi, A.R. Impact of carbonate and heavy metals on micro-structural variations of clayey soils. *Appl. Clay Sci.* **2011**, *52*, 228–234. [[CrossRef](#)]
21. Vippola, M.; Ahmaniemi, S.; Keränen, J.; Vuoristo, P.; Lepistö, T.; Mäntylä, T.; Olsson, E. Aluminum phosphate sealed alumina coating: Characterization of microstructure. *Mater. Sci. Eng. A* **2002**, *323*, 1–8. [[CrossRef](#)]
22. Graeser, S.; Postl, W.; Bojar, H.B.; Armbruster, T.; Raber, T.; Ettinger, K.; Walter, F. Struvite-(K), $\text{KMgPO}_4\cdot 6\text{H}_2\text{O}$, the potassium equivalent of struvite a new mineral. *Eur. J. Miner.* **2008**, *20*, 629–633. [[CrossRef](#)]
23. Lou, K.; Rajapaksha, A.U.; Ok, Y.S.; Chang, S.X. Sorption of copper(II) from synthetic oil sands process-affected water (OSPW) by pine sawdust biochars: Effects of pyrolysis temperature and steam activation. *J. Soil Sediment* **2016**, *16*, 2081–2089. [[CrossRef](#)]
24. Yao, C. Extended and improved Langmuir equation for correlating adsorption equilibrium data. *Sep. Purif. Technol.* **2000**, *19*, 237–242. [[CrossRef](#)]
25. Lord, R.; Sakrabani, R. Ten-year legacy of organic carbon in non-agricultural (brownfield) soils restored using green waste compost exceeds 4 per mille per annum: Benefits and trade-offs of a circular economy approach. *Sci. Total Environ.* **2019**, *686*, 1057–1068. [[CrossRef](#)] [[PubMed](#)]
26. De Souza, C.D.C.B.; Amaral Sobrinho, N.M.B.D.; Lima, E.S.A.; Lima, J.D.O.; Carmo, M.G.F.D.; Garcia, A.C. Relation between changes in organic matter structure of poultry litter and heavy metals solubility during composting. *J. Environ. Manag.* **2019**, *247*, 291–298. [[CrossRef](#)]
27. Guo, X.; Li, C.; Zhu, Q.; Huang, T.; Cai, Y.; Li, N.; Liu, J.; Tan, X. Characterization of dissolved organic matter from biogas residue composting using spectroscopic techniques. *Waste Manag.* **2018**, *78*, 301–309. [[CrossRef](#)]
28. Huang, J.; Huang, Z.; Zhou, J.; Li, C.; Yang, Z.; Ruan, M.; Li, H.; Zhang, X.; Wu, Z.; Qin, X.; et al. Enhancement of heavy metals removal by microbial flocculant produced by *Paenibacillus polymyxa* combined with an insufficient hydroxide precipitation. *Chem. Eng. J.* **2019**, *374*, 880–894. [[CrossRef](#)]
29. Fan, Y.; Zheng, C.; Huo, A.; Wang, Q.; Shen, Z.; Xue, Z.; He, C. Investigating the binding properties between antimony(V) and dissolved organic matter (DOM) under different pH conditions during the soil sorption process using fluorescence and FTIR spectroscopy. *Ecotoxicol. Environ. Saf.* **2019**, *181*, 34–42. [[CrossRef](#)]
30. Iftime, M.M.; Ailiese, G.L.; Ungureanu, E.; Marin, L. Designing chitosan based eco-friendly multifunctional soil conditioner systems with urea controlled release and water retention. *Carbohydr. Polym.* **2019**, *223*, 115040. [[CrossRef](#)]
31. Uchimiya, M.; Bannon, D.I.; Wartelle, L.H. Retention of heavy metals by carboxyl functional groups of biochars in small arms range soil. *J. Agric. Food Chem.* **2012**, *60*, 1798–1809. [[CrossRef](#)]
32. Schilling, M.; Cooper, W.T. Identification of copper binding sites in soil organic matter through chemical modifications and ^{13}C CP-MAS NMR spectroscopy. *Environ. Sci. Technol.* **2004**, *38*, 5059–5063. [[CrossRef](#)]
33. Yang, K.; Miao, G.; Wu, W.; Lin, D.; Pan, B.; Wu, F.; Xing, B. Sorption of Cu^{2+} on humic acids sequentially extracted from a sediment. *Chemosphere* **2015**, *138*, 657–663. [[CrossRef](#)]
34. Karlsson, T.; Elgh-Dalgren, K.; Skjällberg, U.; Sveriges, L. Modeling copper(II) complexation in a peat soil based on spectroscopic structural information. *Soil Sci. Soc. Am. J.* **2008**, *72*, 1286. [[CrossRef](#)]
35. Shi, J.; Wu, Q.; Zheng, C.; Yang, J. The interaction between particulate organic matter and copper, zinc in paddy soil. *Environ. Pollut.* **2018**, *243*, 1394–1402. [[CrossRef](#)]
36. Strawn, D.G.; Baker, L.L. Speciation of Cu in a contaminated agricultural soil measured by XAFS, $\mu\text{-XAFS}$, and $\mu\text{-XRF}$. *Environ. Sci. Technol.* **2008**, *42*, 37–42. [[CrossRef](#)] [[PubMed](#)]
37. Town, R.M.; Powell, H. Ion-selective electrode potentiometric studies on the complexation of copper(ii) by soil-derived humic and fulvic-acids. *Anal. Chim. Acta.* **1993**, *279*, 221–233. [[CrossRef](#)]
38. Yang, R.; Tao, J.; Huang, Q.; Tie, B.; Lei, M.; Yang, Y.; Du, H. Co-adsorption of Cd(II) and Sb(III) by ferrihydrite: A combined XPS and ITC study. *J. Soil Sediment* **2019**, *19*, 1319–1327. [[CrossRef](#)]

39. Alam, M.S.; Gorman-Lewis, D.; Chen, N.; Flynn, S.L.; Ok, Y.S.; Konhauser, K.O.; Alessi, D.S. Thermodynamic Analysis of Nickel(II) and Zinc(II) Adsorption to Biochar. *Environ. Sci. Technol.* **2018**, *52*, 6246–6255. [[CrossRef](#)]
40. Chen, J.W.; Jiao, Y.; Wang, X.D. Thermodynamic studies on gas-based reduction of vanadium titanomagnetite pellets. *Int. J. Miner. Metall. Mater.* **2019**, *26*, 822–830. [[CrossRef](#)]
41. Makowska, J.; Wyrzykowski, D.; Pilarski, B.; Neubauer, D.; Kamysz, E.; Tesmar, A.; Chmurzyński, L. Copper(II) coordination properties of GxG peptides: Key role of side chains of central residues on coordination of formed systems; combined potentiometric and ITC studies. *J. Chem. Thermodyn.* **2019**, *128*, 336–343. [[CrossRef](#)]
42. North, M.L.; Wilcox, D.E. The shift from entropic Cu²⁺ binding to enthalpic Cu⁺ binding determines the reduction thermodynamics of blue copper proteins. *J. Am. Chem. Soc.* **2019**, *141*, 14329–14339. [[CrossRef](#)] [[PubMed](#)]
43. Du, H.; Huang, Q.; Zhou, M.; Tie, B.; Lei, M.; Wei, X.; Liu, X.; Yang, Y. Sorption of Cu(II) by Al hydroxide organo-mineral coprecipitates: Microcalorimetry and NanoSIMS observations. *Chem. Geol.* **2018**, *499*, 165–171. [[CrossRef](#)]
44. Fan, J.; Zeng, Y.; Sun, J. The transformation and migration of selenium in soil under different Eh conditions. *J. Soil Sediment* **2018**, *18*, 2935–2947. [[CrossRef](#)]
45. Gerin, P.A.; Genet, M.J.; Herbillon, A.J.; Delvaux, B. Surface analysis of soil material by X-ray photoelectron spectroscopy. *Eur. J. Soil Sci.* **2003**, *54*, 589–603. [[CrossRef](#)]
46. Yao, T.; Chen, R.; Feng, Y.; Lin, X. Application of bioinformatics to spectral analysis: Soil organic carbon structure distinguished by X-ray photoelectron spectroscopy. *Anal. Bioanal. Chem.* **2019**, *411*, 2481–2485. [[CrossRef](#)]
47. Huang, Z.; Huang, Z.; Feng, L.; Luo, X.; Wu, P.; Cui, L.; Mao, X. Modified cellulose by polyethyleneimine and ethylenediamine with induced Cu(II) and Pb(II) adsorption potentialities. *Carbohydr. Polym.* **2018**, *202*, 470–478. [[CrossRef](#)] [[PubMed](#)]
48. Huang, L.; Ko, T. Feasibility application of Cu-contaminated soil on the removal of H₂S from hot coal gas. *Mater. Trans.* **2015**, *56*, 445–449. [[CrossRef](#)]
49. Li, C.; Yan, A.; Xie, X.; Zhang, J. Adsorption of Cu(II) on soil humin: Batch and spectroscopy studies. *Environ. Earth. Sci.* **2019**, *78*, 487. [[CrossRef](#)]
50. Fulda, B.; Voegelin, A.; Ehlert, K.; Kretzschmar, R. Redox transformation, solid phase speciation and solution dynamics of copper during soil reduction and reoxidation as affected by sulfate availability. *Geochim. Cosmochim. Acta* **2013**, *123*, 385–402. [[CrossRef](#)]
51. Qi, Y.; Zhu, J.; Fu, Q.; Hu, H.; Rong, X.; Huang, Q. Characterization and Cu sorption properties of humic acid from the decomposition of rice straw. *Environ. Sci. Pollut. R.* **2017**, *24*, 23744–23752. [[CrossRef](#)]
52. Boiocchi, M.; Bonizzoni, M.; Ciarrocchi, C.; Fabbri, L.; Invernici, M.; Licchelli, M. Anion recognition in water, including sulfate, by a bicyclam bimetallic receptor: A process governed by the enthalpy/entropy compensatory relationship. *Chem. Eur. J.* **2018**, *24*, 5659–5666. [[CrossRef](#)] [[PubMed](#)]
53. Xu, J.; Koopal, L.K.; Fang, L.; Xiong, J.; Tan, W. Proton and copper binding to humic acids analyzed by XAFS Spectroscopy and isothermal titration calorimetry. *Environ. Sci. Technol.* **2018**, *52*, 4099–4107. [[CrossRef](#)] [[PubMed](#)]
54. Cai, Y.F.; Xue, J.Y. A study of adsorption and absorption mechanisms of copper in palygorskite. *Clay Miner.* **2008**, *43*, 195–203. [[CrossRef](#)]
55. Jefferson, W.A.; Hu, C.; Liu, H.; Qu, J. Reaction of aqueous Cu–Citrate with MnO₂ birnessite: Characterization of Mn dissolution, oxidation products and surface interactions. *Chemosphere* **2015**, *119*, 1–7. [[CrossRef](#)]
56. Ma, L.; Xu, R.; Jiang, J. Adsorption and desorption of Cu(II) and Pb(II) in paddy soils cultivated for various years in the subtropical China. *J. Environ. Sci.* **2010**, *22*, 689–695. [[CrossRef](#)] [[PubMed](#)]
57. Wang, R.; Zhu, X.; Qian, W.; Tang, H.; Jiang, J.; Yu, Y.; Xu, R. Effect of tea polyphenols on copper adsorption and manganese release in two variable-charge soils. *J. Geochem. Explor.* **2018**, *190*, 374–380. [[CrossRef](#)]

Disclaimer/Publisher’s Note: The statements, opinions and data contained in all publications are solely those of the individual author(s) and contributor(s) and not of MDPI and/or the editor(s). MDPI and/or the editor(s) disclaim responsibility for any injury to people or property resulting from any ideas, methods, instructions or products referred to in the content.